PCCP

Cite this: *Phys. Chem. Chem. Phys.*, 2011, **13**, 18355–18364

www.rsc.org/pccp

PAPER

Multi-electron spectroscopy: Auger decays of the argon 2s hole

Pascal Lablanquie,*[ab] Saana-Maija Huttula,[abc] Marko Huttula,[abc] Lidija Andric,[abd] Jérôme Palaudoux,[ab] John H. D. Eland,[e] Yasumasa Hikosaka,[f] Eiji Shigemasa,[g] Kenji Ito[h] and Francis Penent[ab]

Received 13th May 2011, Accepted 27th June 2011
DOI: 10.1039/c1cp21546a

Auger decay of an inner shell hole is an efficient way to create multiply charged ions in the gas phase. We illustrate this with the example of the argon 2s decay, and show that multi-electron coincidence spectroscopy between the 2s photoelectron and all released Auger electrons leads to a complete reconstruction of the Ar 2s decay cascade. Spectra of the intermediate and final Ar^{n+} states are obtained and are compared with a theoretical model.

1. Auger electron spectroscopy: a tool to study multiply charged ions

A Conventional Auger electron spectroscopy *versus* Auger multi-electron coincidence spectroscopy

Conventional Auger electron spectroscopy is widely used in surface science as a diagnostic of material composition[1,2] since Auger electrons are element specific. In the gas phase a M^{2+} doubly charged species is created after single Auger decay of the inner shell hole, and indeed properties of dications have been widely studied by conventional Auger spectroscopy. A vast literature and useful reviews exist[3–5] and only a few examples can be cited here. Mehlhorn[6,7] was a pioneer in developing Auger spectroscopy in the 60s, and together with the groups of K. Siegbahn[8,9] and of Carlson and Krause[10,11] they explored dicationic states both in atoms[6,9] and in molecules.[6,8,11] The increased use of synchrotron radiation then allowed decisive progress in improving the description of the dicationic states populated by Auger decay. In atoms, this deeper understanding can be illustrated by the examples of Ar^{2+}[12,13] or Kr^{2+}.[7,9,14–16] In molecules, it became possible for instance to test whether the two final holes are localized or not near the initially ionized atom[17] and to establish propensity rules for the Auger process.[18–20] The most recent high resolution studies allow the extraction of dications' vibrational structure, as demonstrated recently in HBr[20] and CO.[21]

However two points limit this use of conventional Auger spectroscopy: firstly Auger spectra contain the overlap of decays from different intermediate states: vibrational, spin–orbit, shake-up or shake-off components of core hole states, or possibly similar core holes from non-equivalent atoms of the same Z (such as in N_2O). As a result it is not always possible to extract information on the final dicationic states, especially for dissociative molecular ones. Secondly triply or higher charged ions can also be produced by Auger decay. This can occur through double Auger decay of a shallow core hole,[10] or from cascade decay of a deeper core hole,[7] and information on these multiply charged ions is diluted in the whole Auger spectrum. Electron–electron coincidence spectroscopies provided the solution to these problems. The first generation of the gas phase photoelectron–Auger electron coincidence experiment appeared in the 90s.[22–25] The major improvement of these further studies was the development of strategies to increase electron–electron coincidence efficiency. These include time of flight (TOF) spectrometers[26–28] which enable simultaneous observation of a large electron energy range, new electrostatic analysers of a large acceptance angle,[29] simultaneous use of several electrostatic[30] or TOF analysers,[26–28,31,32] threshold electron analysers[33–42] which allow a 4π detection of low energy electrons (less than a few tenths of meV) and reaction microscopes which reconstruct photoelectron–Auger electron coincidences from ion recoil.[43,44] These photoelectron–Auger electron and Auger electron–Auger electron coincidences made it possible to study triply charged ions such as Ar^{3+},[27] Kr^{3+}[28] and Xe^{3+}.[28,35] They also revealed details of the spectra of dications and the dynamics of their formation in the Auger process, both in atoms[26,33,34,36,38,39,41] and in molecules.[30–32,37,40,42–44] It was soon realized that photoelectron–Auger electron coincidences probe the resultant dicationic states directly, and that the inherent resolution limit of conventional

[a] *CNRS, LCPMR (UMR 7614), 11 rue Pierre et Marie Curie, 75231 Paris Cedex 05, France. E-mail: pascal.lablanquie@upmc.fr*
[b] *UPMC, Université Paris 06, LCPMR, 11 rue Pierre et Marie Curie, 75231 Paris Cedex 05, France*
[c] *Department of Physics, P.O. Box 3000, 90014 University of Oulu, Finland*
[d] *Université Paris-Est, 5 boulevard Descartes, 77454 Marne-la-ValléeCedex 2, France*
[e] *Department of Chemistry, Oxford University, South Parks Road, Oxford, OX1 3QZ, UK*
[f] *Department of Environmental Science, Niigata University, Niigata 950-2181, Japan*
[g] *UVSOR Facility, Institute for Molecular Science, Okazaki 444-8585, Japan*
[h] *Photon Factory, Institute of Materials Structure Science, Oho, Tsukuba 305-0801, Japan*

Auger spectroscopy due to the finite lifetime of the core hole could be overcome. This property leads to the so called 'Subnatural Linewidth Auger–Photoelectron Coincidence Spectroscopy'.[26,33]

Substantial progress was brought about when magnetic bottle type spectrometers[45] were developed in 2003[46] and implemented for use in synchrotron laboratories;[47] it was then possible to perform efficiently coincidences not only between 2 electrons, but also between 3 or more (up to 5 in practice), giving rise to true multi-electron coincidence spectroscopies. New exciting explorations could then begin. Formation of triply charged ions by double Auger decay was explored in detail in atoms (Xe^{3+},[47,48] Ar^{3+},[49,50] Kr^{3+} [51]) and in molecules (CS_2,[52] CH_4,[53] OCS,[54] HBr[55]). These confirmed for instance that even for the simple Kr^{3+} ground state, the literature value of the triple ionisation energy was in error by 1 eV.[28,51] The molecular studies probed the details of dissociative triply charged potential curves.[55] More sophisticated studies have isolated Auger decays of shake-up (in Ne[56] and N_2[57]) or shake-off states (also called core–valence states) in Ne and N_2,[57,58] and have revealed peculiar excited doubly charged states formed by resonant Auger decay in CO[59] and Ar.[60] The most recent achievement is detection of double core hole formation and identification of highly excited triply charged ions populated by their Auger decay in N_2[61] and NH_3.[62]

B The Ar 2s case

In this paper we selected the Ar 2s example to demonstrate that multi-electron Auger coincidence spectroscopy allows the reconstruction of the full Auger cascade of a deep inner shell hole, and reveals spectroscopic and dynamical information on the Ar^{n+} (n = 2 to 4) final and intermediate states which are populated.

The argon configuration is $1s^22s^22p^6v^8$ where v represents the valence 3s and 3p shells. 2s is the second inner shell level and has a binding energy of 326.25 eV,[63] to be compared with 250.776 and 248.628 eV, respectively, for the $2p_{1/2}$ and $2p_{3/2}$ levels.[64] The 2s hole is characterized by a very short lifetime of 0.290 fs due to the very efficient L_1-$L_{2,3}M$ Coster–Kronig† Auger decay process in which a 2p electron from the same shell fills the 2s hole while a valence shell electron is ejected. This results in an intrinsic lifetime broadening of 2.25 ± 0.5 eV.[63] The first experimental observation of the L_1-$L_{2,3}M$ Auger spectrum was presented by Mehlhorn in 1968.[65] More recent measurements[66] improved intensity estimates but did not bring any improvement in terms of resolution of the core–valence Ar^{2+} $2p^{-1}v^{-1}$ states populated in the decay, because of the large lifetime broadening. It is the use of photoelectron–Auger electron coincidences which could go beyond this limit thanks to the 'Subnatural Linewidth Auger Coincidence Spectroscopy' regime.[33,39]

The distribution of final Ar^{n+} ions populated by the complete 2s cascade decay was calculated[67] and measured by electron–ion coincidence;[68] we will present here the detailed Auger spectra associated with each final charge.

The relatively low kinetic energies of Coster–Kronig transitions and the heavy overlap of the wave functions make the transitions particularly sensitive to the calculation methods. Changes in kinetic energies and potential, where the wave functions are generated, may easily affect the decay rates.[69] The transitions are also sensitive to such effects as the exchange between the continuum electron and the bound electrons[70] and the mixing of final-state channels.[71] We also point out that it is important to use a correlated description of all the Ar^{n+} states involved in order to achieve an accurate description of the phenomena observed.[33,66,69–71]

2. Methods

A Experiment

Experiments were mainly performed on the U56/2 PGM1 beam line[72] of the BESSY-II synchrotron during single bunch operation that provides light pulses of a few tens of ps width every 800.5 ns. Our HERMES (High Energy Resolution Multi-Electron Spectrometer) set-up is a magnetic bottle time-of-flight analyser which has been described in detail before,[51,55] and only points of interest for this experiment will be recalled here. HERMES allows the simultaneous collection of almost all electrons (>95% of 4π solid angle) emitted following ionization of a single atom. A detection efficiency of 50 ± 5% was measured for 0–300 eV electrons, due to the use of a 90% transparency grid in front of a multi-channel plate (MCP) detector with an open area ratio of 60%. The energy resolution of the apparatus, $\Delta E/E$, was estimated to be nearly constant at 1.5% for electrons of $E > 1$ eV, though ΔE was limited to around 20 meV (FWHM) for $E < 1$ eV. Multi-electron coincidence datasets were accumulated for 2 h each at two different photon energies (402 and 334.3 eV), where the photon bandwidths were set to around 30 meV. The electron count rate was maintained at ~5 kHz to minimize random coincidence counts. These are mainly associated with the probability that two Ar atoms are ionised by the same light bunch (with one ionisation event every 250 bunches on average) and can be simulated for single dimension spectra with the aid of non-coincident time-of-flight spectra of all detected electrons.

Complementary experiments were conducted at the undulator beam line BL-16A of the Photon Factory. Single bunch operation of the storage ring provided light pulses of 200 ps width every 624 ns. A mechanical chopper[73] was used to extend the light pulse interval to 12.5 μs; it allowed absolute time of flight measurements and decreased the background (by avoiding pile-up of slow electrons in one period). Such a device was not used in experiments at BESSY, as in the specific case of Ar inner-shell decay the detection of the fast (150–290 eV) Auger electron allows the reconstruction of the absolute times of flight of all electrons of an ionisation event. The experimental setup is a magnetic bottle type analyser similar to the one used in experiments at BESSY and was described previously.[50,60] These complementary experiments were conducted in order to observe with higher statistics the triple

† Definition of the standard Auger notation can be found in ref 1–4. Here, the L_1-$L_{2,3}M$, L_1-MM and $L_{2,3}M$-MMM Auger processes stand, respectively, for the $2s^{-1} \rightarrow 2p^{-1}(3s,3p)^{-1}$, $2s^{-1} \rightarrow (3s,3p)^{-2}$ and $2p^{-1}(3s,3p)^{-1} \rightarrow (3s,3p)^{-3}$ transitions. A Coster–Kronig Auger decay involves participation of an electron from a higher subshell of the same shell as the initial hole.

Auger decay of the Ar 2s hole. The topping-up operation mode of the Photon Factory was essential to provide stable conditions necessary during the 12 h acquisition time. A photon energy of 633 eV was chosen to ensure that the 2s photoelectron was faster than any of the three subsequent Auger electrons of interest. A detector dead time of 15 ns prevents detection of electrons with similar energies but was not critical in the present case.

B Theoretical model

Calculations were performed to describe the Ar^+ $2s^{-1}$ initial state, the Ar^{2+} $2p^{-1}v^{-1}$ or Ar^{2+} v^{-2} states reached in the first Auger step, and the associated transition probabilities. The theoretical predictions were done within the multi-configurational Dirac–Fock formalism by applying the GRASP92 code[74] and RELCI program from RATIP package.[75] The MCDF method is described in detail elsewhere (see *e.g.* ref. 74 and references therein), so only the main principles are reviewed here. In the MCDF method, the atomic state functions (ASFs), characterized by the total angular momentum J_α and parity P_α, are represented in the basis of jj-coupled configuration state functions (CSFs) with the same J_α and parity P_α, as

$$|\Psi_\alpha(P_\alpha J_\alpha)\rangle = \sum_k c_{\alpha k}|\psi_k(P_\alpha J_\alpha)\rangle$$

The mixing coefficients $c_{\alpha k}$ are obtained by diagonalizing the two-electron interaction matrix, which takes the electronic correlations into account. The wave functions are obtained self-consistently using the Dirac–Coulomb Hamiltonian.

For the light atom Ar, the orbital and spin angular momenta of the outer electrons are not strongly interacting. Therefore the coupling conditions are close to LSJ coupling. Thus the inherently jj-coupled ASFs were transformed into the LSJ basis by the unitary transformation between the two bases applying the program LSJ.[76]

The Auger decay intensity is given by

$$n_{f\beta} = \frac{2\pi \sum_{l_{A j_A}} \left| \sum_{\mu\nu} C_{f\mu} C_{\beta\nu} M^{\mu\nu}_{f\beta}(J_f, J_\beta) \right|^2}{P_\beta(J_\beta)} Q_\beta(J_\beta)$$

where $M^{\mu\nu}_{f\beta}(J_f, J_\beta)$ is the Coulomb matrix element $\left\langle \psi_\mu(J_f)\varepsilon_A l_A j_A : J_\beta \left\| \sum_{mn}^{N=1} \frac{1}{r_{mn}} \right\| \psi_\nu(J_\beta) \right\rangle$, $P_\beta(J_\beta)$ is the total decay rate and $Q_\beta(J_\beta)$ is the $|\Psi(J_i)\rangle \rightarrow |\Psi(J_\beta)\rangle$ ionization cross-section. The Auger decay intensities were calculated using the AUGER component from the RATIP package. For more details about the AUGER program see ref. 75 and 77 and references therein. Channel mixing was omitted in our calculations.

3. Reconstruction of the Ar 2s Auger cascades

The complete Ar 2s coincident Auger spectrum is represented in Fig. 1. Examining coincidences with the Ar 2s photoelectron enables us to filter out the 2s Auger electrons which are hidden among 2p and 2p satellite Auger electrons in conventional (non-coincident) Ar Auger spectra.[78] The high sensitivity and the low background reveal for instance weak high energy components in the 240–280 eV range, which have not been reported previously, to the best of our knowledge. They correspond to final Ar^{2+} v^{-2} states and L_1-MM Auger processes.

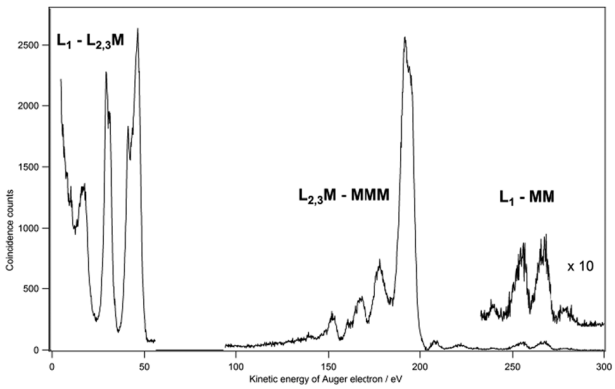

Fig. 1 Complete coincident Auger spectrum associated with the decay of the Ar 2s hole. The Auger electrons were detected in coincidence with the 2s photoelectron at a photon energy of 402 eV; the dead time of the detector prevents the observation of the coincident Auger electrons of energies close to the ~76 eV 2s photoelectron. False coincidences, associated with the weak probability of ionizing another Ar atom in the same light pulse, were modelled and subtracted. The intensity scale is expanded and offset to show the weaker L_1-MM processes.

In the low energy region of the coincident Auger spectrum one recognizes the L_1-$L_{2,3}$M Coster–Kronig lines, with the structures at ~45 eV and ~30 eV associated with the population of the previously observed Ar^{2+} $2p^{-1}3p^{-1}$ and Ar^{2+} $2p^{-1}3s^{-1}$ states.[33,39,65,66] A third structure centred at around 15 eV corresponds to the population of satellite states of the Ar^{2+} $2p^{-1}3p^{-2}nl$ type, which have not been isolated previously in conventional Auger spectra, and were only detected in coincident Auger spectra.[39] They lie on a signal rising towards 0 eV which is associated partly with Auger electrons emitted at the end of the 2s Auger cascade and partly with false coincidences involving low energy secondary electrons emitted from surfaces.

As the Ar^{2+} $2p^{-1}v^{-1}$ states produced by L_1-$L_{2,3}$M Coster–Kronig decay still contain an inner-shell 2p hole, their decay is also observed in coincidence with the 2s photoelectron and gives rise to the structures between 100 and 230 eV. These $L_{2,3}$M-MMM lines were studied by Kylli *et al.*,[78] but their conventional Auger spectra prevented a clear observation of the complete processes.

A Decay of the 2s hole to final Ar^{2+} ions by emission of a single Auger electron

Final Ar^{2+} states are populated by L_1-MM Auger decays, as seen in the high energy region of Fig. 1 and expanded in Fig. 2. The experiment is affected by the ~4 eV resolution of the analyser for 250 eV electrons, and by the 2s line width of 2.25 eV.

Single configuration (SC) calculations describe the ionized $2s^{-1}$ states well, but for the Auger final states multi-configuration (MC) calculations are needed. The MC calculations for the lowest binding energy doubly ionized states included

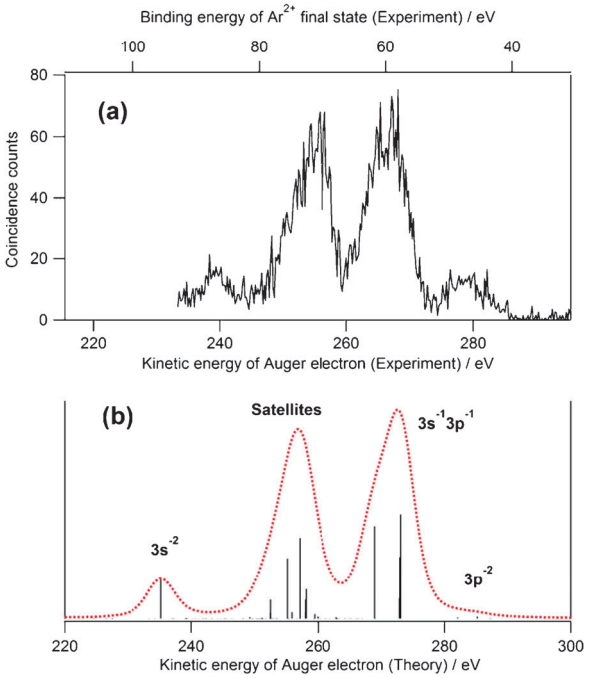

Fig. 2 Ar 2s Auger spectrum associated with decay to form Ar^{2+} final states: (a) experiment, (b) our calculations (bars) convoluted with a Voigt profile to simulate experimental conditions (red dotted lines), see the text. Note that the experiment and theory Auger energy scales are shifted for easier comparison. This is because theory slightly overestimates these energies, while finding good relative values.

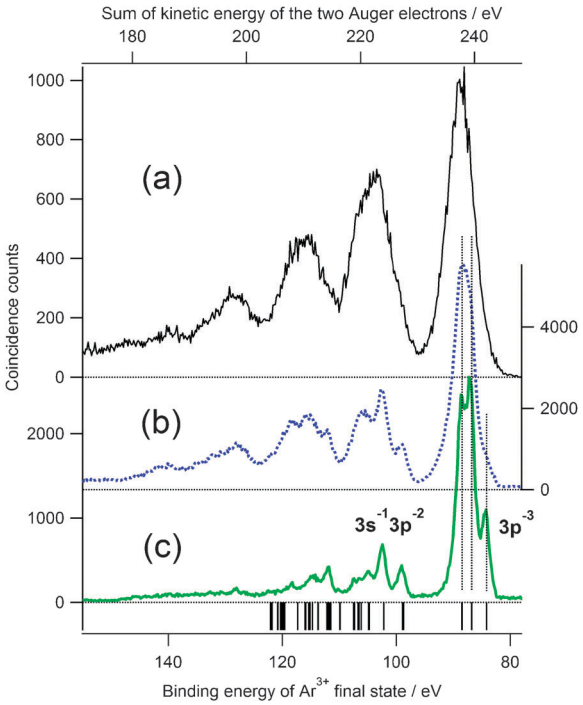

Fig. 3 Ar^{3+} states populated by double Auger decay of a 2s hole in (a) and (b) or of a $2p_{3/2}$ hole in (c). (a) is obtained at $h\nu = 402$ eV by plotting the histogram of the sum of the kinetic energies (top axis) of the two Auger electrons coincident with a 2s photoelectron. Ar^{3+} binding energies in the bottom axis are retrieved by eqn (1). Curves (b) and (c) were obtained at $h\nu = 334.3$ eV by considering three electron coincidences (a 2s or $2p_{3/2}$ photoelectron + two Auger) and eqn (2). The top scale applies to (a) only while the bottom scale applies to all three curves. (c) is similar to Fig. 1(b) in ref. 50, obtained at a lower photon energy for the total 2p decay; it is also similar to the one obtained here for the $2p_{1/2}$ decay (not shown). Vertical bars at the bottom indicate Ar^{3+} levels from the literature.[82]

the non-relativistic configurations $(3s3p)^6$, $(3s3p)^5 3d^1$, $3s^2 3p^3(4s,4d)^1$, $3s^0 3p^4(3d,4s)^2$ and $3s^1 3p^4 4s^1$. The theoretical prediction is shown in Fig. 2. The calculated energies and intensities have been convoluted with a Voigt profile (dotted red line) using a Gaussian line width of 4 eV and a Lorentzian of 2.25 eV to simulate the experiment. Excellent agreement is reached. The spectrum is dominated by Ar^{2+} $3s^{-1}3p^{-1}$ and Ar^{2+} satellites of the $3s^2 3p^{-3}$nl configuration. The Ar^{2+} $3s^{-2}$ final state is clearly identified while Ar^{2+} $3p^{-2}$ states are predicted to be almost absent, and are observed only with a very weak intensity. This suggests that the dominant L_1-MM process is filling of the 2s hole by a 3s electron, with ejection of a valence 3s or 3p electron. Note that resolution of the individual Ar^{2+} final states is in principle experimentally feasible in the 'Subnatural Linewidth Auger Coincidence Spectroscopy' regime but would require a higher resolution apparatus than ours.

B Decay of the 2s hole to final Ar^{3+} ions by emission of two Auger electrons

Ar 2s decay to Ar^{3+} final states is probed by three electron coincidences between the 2s photoelectron and the two Auger electrons. Fig. 3(a) shows the sum $E_{A'} + E_{A''}$ of the kinetic energy of these two Auger electrons. The binding energy $E_b(Ar^{3+})$ of the final Ar^{3+} state is then retrieved from:

$$E_b(Ar^{3+}) = E_b(2s) - (E_{A'} + E_{A''}) \quad (1)$$

Resolution in Fig. 3(a) is hard to simulate as it includes a combination of the energy resolution on each Auger electron and the 2s lifetime broadening, but can be estimated as ~4–5 eV. The 2s lifetime broadening contribution can be removed in the 'Subnatural Linewidth Auger regime' in Fig. 3(b) by considering the following energy balance:

$$E_b(Ar^{3+}) = h\nu - E_k(2s) - (E_{A'} + E_{A''}) \quad (2)$$

where $E_k(2s)$ is the kinetic energy of the 2s photoelectron. Resolution in Fig. 3(b) is then purely experimental and amounts to ~3 eV. The lower kinetic energy of the 2s photoelectron due to the use of 334.3 eV photons also contributes to the improvement of the energy resolution. The five lowest final Ar^{3+} states (vertical bars in Fig. 3) are then almost resolved. Comparison with a similar spectrum but associated with the double Auger decay of the $2p_{3/2}$ hole in Fig. 3(c) shows that relative intensities are significantly different: the Ar 2s double Auger decay produces more excited Ar^{3+} levels, implying an increased proportion of 3s holes. The intensities of the ^4S, ^2D and ^2P components of the $3p^{-3}$ electronic levels (located just below 90 eV binding energy) also differ, with population of the highest energy ^2P level being preferred in 2s decay. Note that coincidence count rates in Fig. 3(b) and (c) are obtained from the same data set and can be directly compared; they demonstrate that at this photon

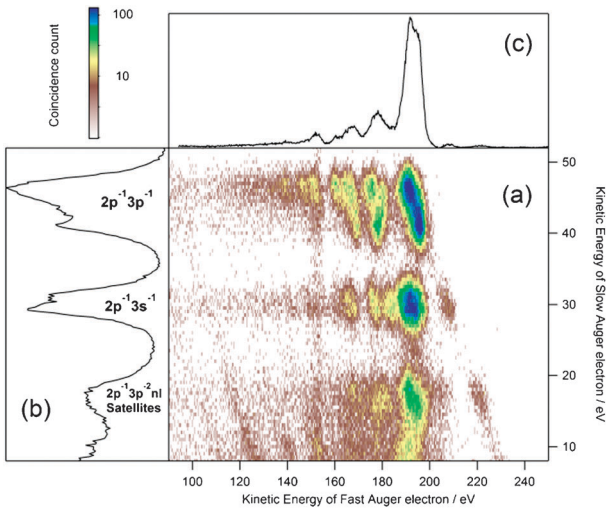

Fig. 4 (a) Two dimensional plot of energy correlation between the two Auger electrons emitted upon 2s double Auger decay. All three-electron coincidences between a 2s photoelectron and two Auger electrons in the dataset obtained at $h\nu = 402$ eV are considered. (b) and (c) show projections of the two dimensional plot in (a) and are similar to Fig. 1. The faint vertical line at 153 eV originates from false coincidences with 2p photoelectrons, which have not been subtracted in (a) but were subtracted in the projection (c) and in Fig. 1.

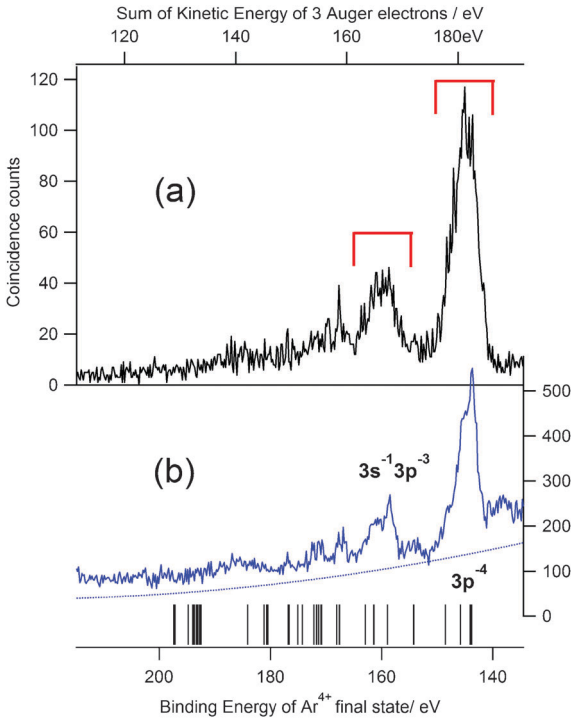

Fig. 5 Ar^{4+} states populated by triple Auger decay of a 2s hole. (a) is obtained at $h\nu = 402$ eV by considering the sum of the kinetic energies of the three Auger electrons coincident with a 2s photoelectron. Ar^{4+} binding energies are retrieved by eqn (1a). Curve (b) was obtained at $h\nu = 334.3$ eV by considering four electron coincidences (a 2s photoelectron + three Auger) and eqn (2a); peaks appear on a rising background of false coincidences (dotted blue line). The top scale applies to (a) only while the bottom scale applies to both curves. Vertical bars at the bottom indicate Ar^{4+} levels from the literature.[82] Brackets indicate the energy ranges used in further analysis (Fig. 7).

energy Ar^{3+} formation is 4–5 times more intense by 2s double Auger decay than by $2p_{3/2}$ double Auger decay.

Energy correlations between the two Auger electrons are presented in Fig. 4(a). They show the connection between the L_1-$L_{2,3}M$ Coster–Kronig path (b) and the subsequent $L_{2,3}M$-MMM decay (c). The coincidence map (a) is dominated by islands which demonstrate that Ar 2s double Auger decay is essentially a cascade process with single Auger decay of the Ar^{2+} $2p^{-1}v^{-1}$ core–valence intermediate states populated by the initial L_1-$L_{2,3}$ MCoster–Kronig decay. In this representation, formation of a given final Ar^{3+} state necessarily appears on a diagonal line with a fixed Auger energy sum. One such diagonal is seen with coincidence islands at (193 eV, 43 eV), (208 eV, 30 eV) and (220 eV, 17 eV) and traces Ar^{3+} $3p^{-3}$ formation. One deduces that Ar^{2+} $2p^{-1}3p^{-1}$ states decay preferentially to populate Ar^{3+} $3p^{-3}$ while Ar^{2+} $2p^{-1}3s^{-1}$ ones rarely do so, but prefer to decay into Ar^{3+} $3s^{-1}3p^{-2}$ levels. This demonstrates the origin of the weak peaks at 208 and 220 eV in Fig. 1, which come from the participator Auger decay of core–valence Ar^{2+} states to the ground Ar^{3+} $3p^{-3}$ levels.

C Decay of the 2s hole to final Ar^{4+} ions by emission of three Auger electrons

Ar 2s decay to Ar^{4+} final states is probed by four electron coincidences between the 2s photoelectron and the three Auger electrons. The procedure is similar to the one described in the previous paragraph for the double Auger decay, but with an extra Auger electron. Eqn (1) and (2) thus become:

$$E_b(Ar^{4+}) = E_b(2s) - (E_{A'} + E_{A''} + E_{A'''}) \quad (1a)$$

$$E_b(Ar^{4+}) = h\nu - E_k(2s) - (E_{A'} + E_{A''} + E_{A'''}) \quad (2a)$$

Fig. 5(a) and (b) show that the decay mainly populates the Ar^{4+} $3p^{-4}$ multiplet (and preferentially the ground ^3P level) and that the excited Ar^{4+} $3s^{-1}3p^{-3}$ states are only weakly populated. It was not possible to compare this process with triple Auger decays of the 2p hole states. Although those processes exist[49] they are of too low probability to allow determination of the population of the Ar^{4+} $3p^{-4}$ final states.

The representation of energy correlations between the three Auger electrons is in general a three dimensional problem, but can be simplified to a two dimensional one if we consider a given final Ar^{4+} state for which $E_{A'} + E_{A''} + E_{A'''} = E_{Sum}$ is constant. In this specific case, within our resolution, we observe two different Ar^{4+} states: $3p^{-4}$ and $3s^{-1}3p^{-3}$. We will use a variant of Dalitz plots to visualize energy correlations in these two cases.

Dalitz plots were introduced in nuclear physics[79] to represent three-particle breakup, and have been widely applied in molecular dynamics (see for instance).[80,81,83] Their definition is a purely geometric one depicted in Fig. 6. Let us consider a distribution of 3 electrons e_i whose kinetic energies E_i satisfy: $E_a + E_b + E_c = E_{Sum} =$ constant. Their distribution can be represented using an equilateral triangle of height E_{Sum} by considering the point at distances (E_a, E_b, E_c) from the three sides of the triangle. All representative points can be included

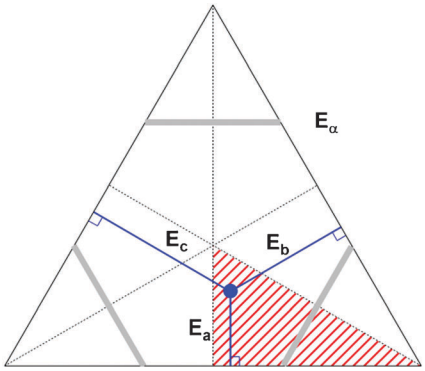

Fig. 6 A variant of Dalitz plots to represent energy correlation between three electrons such as $E_a + E_b + E_c = E_{Sum}$ = constant. The full plot is constructed by geometrical transformation of the (red) hatched triangle. The grey lines depict a cascade process in which an electron of fixed energy E_α is released (see the text).

in the sub-triangle shown with a hatched (red) pattern, for which $E_a < E_b < E_c$. The full Dalitz plot is obtained by the six permutations of the (E_a, E_b, E_c) triplet and is constructed by simple geometrical transformation of the hatched (red) lower right triangle (reflection symmetries with respect to the triangle heights). The strength of such a Dalitz representation is that all three electrons are treated on equal footing. Properties that will be useful in this study are:

- projection of the triangle on one of its heights gives the energy distribution of the energy E_i of any of the three electrons;
- if we consider a cascade process in which an electron of fixed energy E_α is emitted, it will appear as three lines at distances E_α from the sides, the energy sharing between the remaining two electrons being visualized by the density along the line.

Note that this representation differs from the original Dalitz plots[79] where momentum conservation in three-particle breakup imposes the restriction that all data points must lie within the circle included in the equilateral triangle. No such restriction exists here as we deal with a five-particle breakup (an Ar^{4+} ion, a 2s photoelectron and three Auger electrons).

Energy correlations between the three Auger electrons are depicted in Fig. 7(a) and (b) when the final states are, respectively, Ar^{4+} $3p^{-4}$ and $3s^{-1}3p^{-3}$. E_{Sum} was chosen in the corresponding two bands of Fig. 5(a). The plots have been scaled to the mean value for E_{Sum}. Lines appear clearly and reveal the dominant contribution of cascade processes. The nature of these can be found by considering the energy distributions of any of the Auger electrons, given in Fig. 7(c) and (d): one observes the characteristic L_1-$L_{2,3}M$ Coster–Kronig lines in Fig. 1 at ~45 and ~30 eV. The Ar 2s triple Auger decay is thus a cascade process in which a first Coster–Kronig decay populates Ar^{2+} $2p^{-1}v^{-1}$ core–valence intermediate states which then further decay by double Auger emission. As noted previously, energy sharing between these two Auger electrons emitted in the last step of the cascade is revealed by the intensity along the lines on the Dalitz plot. An equivalent, but more informative, representation is displayed in Fig. 8. It shows the energy of one of the last two Auger electrons of the triple Auger cascade. Care must be taken

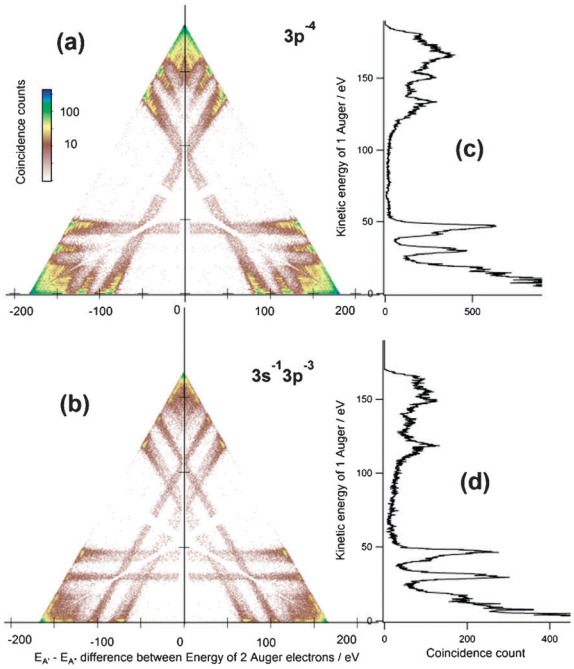

Fig. 7 (a) and (b) Dalitz plots showing the energy correlation between the three Auger electrons emitted upon triple Auger decay of a 2s hole reaching, respectively, an Ar^{4+} $3p^{-4}$ or $3s^{-1}3p^{-3}$ state. (c) and (d) are the projections of the triangles on the y axis, giving the energy distribution of one of the emitted Auger electrons. The white triangular bands at the border of the 6 constituent triangles (see Fig. 6) arise from the 15 ns detector dead time, which forbids detection of electrons of close energies. Photon energy was 633 eV. False coincidences come mainly from low energy secondary electrons of less than a few eV. They appear on the summit of the triangle and have not been subtracted.

in the interpretation of these spectra because the different associated lines in Fig. 7 cross, which means that the different processes cannot always be separated; this is the origin of the peaks at ~30 eV in Fig. 8(a) and ~43 and 106 eV in Fig. 8(b). Nevertheless Fig. 7 and 8 reveal that the double Auger decay of the core–valence Ar^{2+} $2p^{-1}v^{-1}$ states is dominantly a cascade process, with characteristic low energy electrons (<10 eV) being emitted in the last step of the cascade. Direct double Auger paths in which the two Auger electrons share the available energy continuously are also present, as seen from the smooth intensity distribution in Fig. 8 and along the lines in the Dalitz plots of Fig. 7. Interestingly, the direct double Auger decay of the Ar^{2+} $2p^{-1}3s^{-1}$ intermediates to final Ar^{4+} $3p^{-4}$ states is the only path absent.

D Summary: final Ar^{n+} states reached by the 2s hole decay

The probability to end up in an Ar^{n+} ion after completion of the 2s decay cascade is given in Table 1. It is extracted by direct comparison of the coincidence counts in Fig. 2(a), 3(a) and 5(a), which are plotted with the same bin size and obtained from the same data set at $h\nu$ = 402 eV. Note that decay to final Ar^{5+} and Ar^{6+} ions is possible, as the threshold for their formation is given in the literature at 218.94 and 309.94 eV, respectively,[82] that is below the Ar 2s level, but only a weak formation of Ar^{5+} ions was detected. Our experimental values

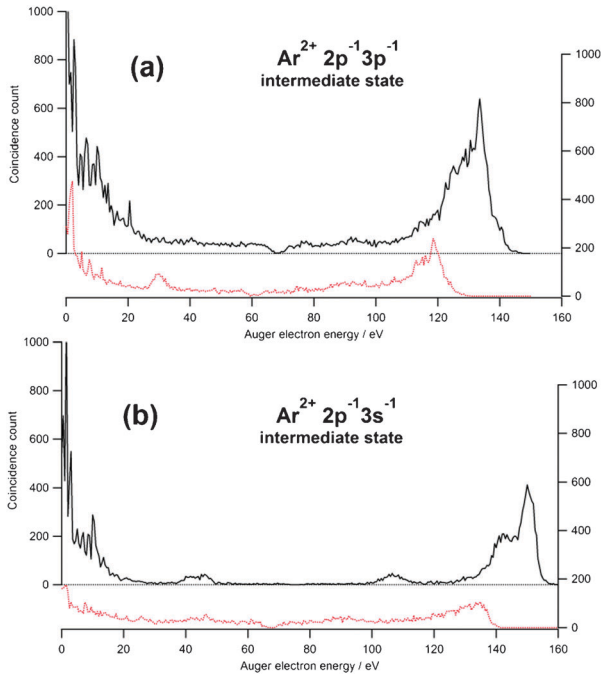

Fig. 8 Energy distribution of the last two electrons emitted in the cascade triple Auger decay of a 2s hole. Intermediate Ar^{2+} $2p^{-1}3p^{-1}$ or $2p^{-1}3s^{-1}$ states are selected in (a) and (b). (Black) solid lines and (red) dotted lines correspond, respectively, to final Ar^{4+} $3p^{-4}$ and $3s^{-1}3p^{-3}$ states. These distributions are retrieved from intensities along the lines in the Dalitz plots of Fig. 7.

Table 1 Relative abundances of multiply charged Ar^{n+} ions produced by de-excitation of the Ar 2s hole. Values are given in %

Final ionic charge	Experiment	Theory	Theory[67]	Exp.[68]
+1	—		0	0
+2	3	5	4.2	1
+3	89	95	93.4	89
+4	8		2.5	10
+5	0.3		0	—

compare well with our theoretical estimates, as we found that in the first step the 2s hole decay involves either valence electrons in a L_1-MM process or 2p electrons in a Coster–Kronig path. Theoretical values are defined by comparing the transition probabilities towards valence double hole states and core + valence hole states from an overall MC calculation including the configurations $2p^5(3s3p)^7$, $2p^53s^23p^4nd$, n = 3–4, $2p^6(3s3p)^6$ and $2p^63s^23p^3(4s,3d)^1$. Our experimental values are also in satisfactory agreement with the ones obtained by Brunken *et al.*[68] in a 2s electron/ion coincidence experiment, and with theoretical estimates by Kochur *et al.*[67] Note that the L_1-M radiative decay of the 2s hole to final Ar^+ ions was studied in ref. 63, but its probability is expected to be very weak and has not been measured to the best of our knowledge.

4. Resolving the Ar^{2+} $2p^{-1}$ $(3s, 3p)^{-1}$ core–valence states formed in the first step of the Ar 2s decay

The first step of Ar 2s hole decay is dominantly the Coster–Kronig process populating core–valence Ar^{2+} $2p^{-1}v^{-1}$ intermediate states. Our aim now is to extract detailed spectroscopic information on these states. The method, 'Subnatural Linewidth Auger–Photoelectron Coincidence Spectroscopy', is well known[26,33] and consists in observing in Fig. 9(a) energy correlations between the 2s photoelectron in (b) and the Coster–Kronig electrons in (c). The photon energy was 334.3 eV, which is only ~8 eV above the 2s threshold. Strong post collision interaction (PCI) distorts the photoelectron and the Auger lines. Clear diagonal lines appear in Fig. 9(a); they reveal the final Ar^{2+} $2p^{-1}v^{-1}$ states. These lines clearly extend further than the 2s photoelectron zone, which demonstrates that the same Ar^{2+} core–valence states can be formed by 2s decay or by core–valence double ionisation, though with different relative intensities. This also shows that in fact the 2s decay should be considered as a resonance in the core–valence double photoionisation process:

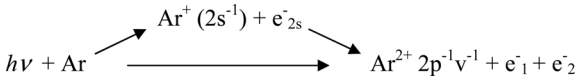

(3)

where (e_1^-, e_2^-) can be the (2s photoelectron, Auger electron) pair or the pair (e_{Ph1}^-, e_{Ph2}^-) of photoelectrons from core–valence double photoionization. Core–valence double photoionisation has been much studied, especially with magnetic bottle spectrometers,[52,57,58,84] and was previously detected for Ar.[33,78] Energy balance from eqn (3) gives:

$$E_b(Ar^{2+}2p^{-1}v^{-1}) = h\nu - E_k(e_1^-) - E_k(e_2^-) \quad (4)$$

Using this relation, Fig. 10(b) reveals the energies and intensities of the Ar^{2+} $2p^{-1}v^{-1}$ states populated by 2s decay.

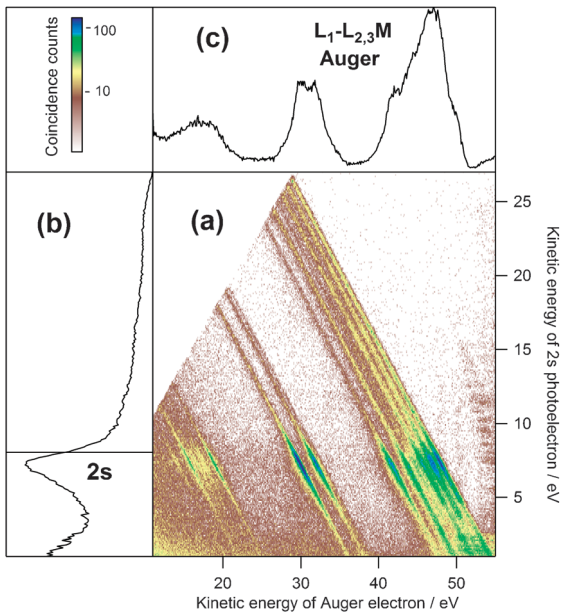

Fig. 9 (a) Energy correlation between the 2s photoelectron projected as (b) and the L_1-$L_{2,3}$M Coster–Kronig Auger electrons projected as (c). The use of the 334.3 eV photon energy causes a strong PCI distortion of the Auger (compare Fig. 1 and 4(b)) and photoelectron lines. The 2s photoelectron is slowed down with respect to its nominal value (black bar).

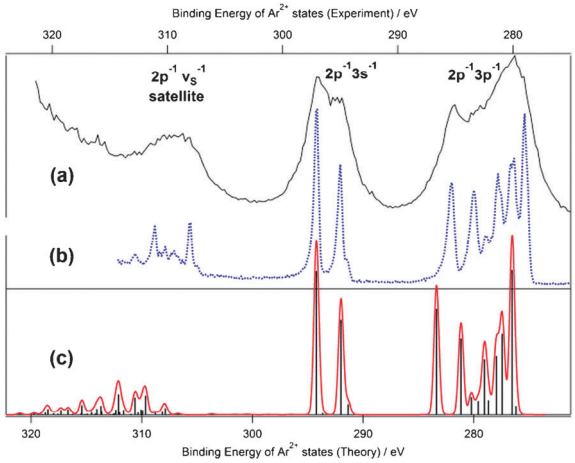

Fig. 10 Ar^{2+} $2p^{-1}v^{-1}$ core–valence states populated by 2s hole decay. (a) is obtained from the Auger spectrum in Fig. 1. (b) is deduced from relation (4) and data in Fig. 9, using a selection range of 4 to 10 eV for the 2s photoelectron. (c) is deduced from our theoretical model (bars) convoluted with 500 meV Gaussian profiles to simulate experimental resolution. Note that PCI distortion due to the decay of the Ar^{2+} $2p^{-1}v^{-1}$ states causes asymmetry in the experimental spectrum; this effect was not included in (c).

It is compared in Fig. 10(a) with the spectrum based on the Ar 2s Auger lines alone. The figure demonstrates clearly how coincidence Auger spectroscopy can allow one to get rid of the lifetime broadening intrinsic to conventional Auger spectroscopy, as was explained previously. Good agreement is found with our theoretical predictions in Fig. 10(c) and Table 2. The transition probabilities were calculated by using a single configuration calculation for the Ar 2s ionized state and the MC calculation for the final states including the non-relativistic configurations $2p^5(3s3p)^7$ and $2p^53s^23p^4nd$, n = 3–4. The ratio of intensities between the $2p^{-1}3s^{-1}$ and the $2p^{-1}3p^{-1}$ lines has been of interest as a sensitive probe of the validity of the description of the Ar^{n+} states involved.[65,66,69–71] On the experimental side, Mehlhorn's first measurement of this ratio gave 0.26,[65] later revised to 0.37.[66] A more recent estimate from conventional Auger spectroscopy gave 0.30 ± 0.02.[66] Our experimental measure gives 0.37, which is in perfect agreement with the revised value of Mehlhorn; we note that an advantage of the magnetic bottle spectrometer is that no correction for transmission of the analyser is needed contrary to ref. 66 so that our estimate should be more reliable. This value is also in good agreement with our theoretical estimate of 0.435. One observes also in Fig. 10 and in Table 2 that states of higher binding energy are weakly populated; they are assigned to Ar^{2+} $2p^{-1}v_s^{-1}$ satellite states of the $2p^{-1}3p^{-2}nl$ configuration. Our theoretical model finds also such lines with intensities in line with experimental observations, but fails in assigning individual lines (see Fig. 10(c)).

Table 2 Spectroscopy of the Ar core–valence states and intensities for their formation by Auger decay of a 2s hole. Experimental values are obtained from a fit of Fig. 10(b) using asymmetrical line shapes

Assignment	Theory energy/eV	Intensity	Experiment energy/eV	Intensity
$2p^{-1}3p^{-1}$ ($^1P_1$)	276.954	6.4	—	—
$2p^{-1}3p^{-1}$ ($^3D_3$)	277.284	100.0	278.9	100
$2p^{-1}3p^{-1}$ ($^3D_2$)	278.149	55.8	279.9	71
$2p^{-1}3p^{-1}$ ($^3S_1$)	278.656	40.5		
$2p^{-1}3p^{-1}$ ($^3P_2$)	279.339	10.2	280.4	29
$2p^{-1}3p^{-1}$ ($^3D_1$)	279.693	38.2	281.2	59
$2p^{-1}3p^{-1}$ ($^3P_0$)	280.235	9.7	282.5	29
$2p^{-1}3p^{-1}$ ($^3P_1$)	280.828	12.3		
$2p^{-1}3p^{-1}$ ($^1D_2$)	281.721	52.4	283.3	60
$2p^{-1}3p^{-1}$ ($^1S_0$)	283.849	73.3	285.3	66
$2p^{-1}3s^{-1}$ ($^3P_2$)	291.528	7.6	294.3	6
$2p^{-1}3s^{-1}$ ($^3P_1$)	292.142	65.9	294.9	60
$2p^{-1}3s^{-1}$ ($^3P_0$)	293.740	1.3	—	—
$2p^{-1}3s^{-1}$ ($^1P_1$)	294.273	98.6	297.0	86
			310.3	15
$2p^{-1}v_S^{-1}$			311.1	9
Satellites			312.8	4

5. Conclusion

We have shown using the Ar 2s example that multi-electron coincidence Auger spectroscopy (where coincidences between the photoelectron and all subsequent Auger electrons are recorded) can provide important information on multiply charged ions. The full cascade decay of the Ar 2s hole has been reconstructed and found to populate Ar^{n+} ions with n = 2 to 5. A variant of Dalitz plots was used to describe the 2s triple Auger decay to Ar^{4+} states. Special emphasis was put on the description of the $Ar^{2+}2p^{-1}v^{-1}$ core–valence states, produced in the first step of the 2s hole decay (L_1-$L_{2,3}$M Coster–Kronig decay). It is also shown that the 2.25 eV 2s lifetime broadening can be eliminated thanks to the coincidence method. Resolution on the Ar^{n+} ion states is then purely experimental and could in principle be improved with an apparatus of better experimental resolution.

Acknowledgements

We would like to dedicate this paper to the memory of Professor W. Mehlhorn who developed Auger spectroscopy and initiated Ar 2s studies.

Experiments were done with the approval of Advisory Committees: Projects No. 2008-1-70762 in BESSY and No. 2008G529 in PF. We are greatly indebted to B. Zada and W. Mahler (BESSY) and to K. Amemiya (PF) for their guidance on the beam lines. Financial support is acknowledged from CNRS (PICS No. 5364), Research Council for Natural Sciences of the Academy of Finland and from the European Community, Research Infrastructure Action under the FP6 "Structuring European research Area" Programme (contract R II 3-CT-2004-506008).

Notes and references

1 C. C. Chang, *Surf. Sci.*, 1971, **25**, 53.
2 D. Chattarji, *The theory of Auger transitions*, Academic Press, 1976, ISBN: 0-12-169850-5.
3 E. H. S. Burhopand and W. N. Asaad, *Adv. At. Mol. Phys.*, 1972, **8**, 163.
4 T. A. Carlson, *Photoelectron and Auger spectroscopy*, Plenum press, 1975 ISBN: 0-306-33901-3.
5 W. Mehlhorn, *J. Electron Spectrosc. Relat. Phenom.*, 1998, **93**, 1.
6 W. Mehlhorn, *Z. Phys.*, 1960, **160**, 247.
7 W. Mehlhorn, *Phys. Lett.*, 1965, **15**, 46; W. Mehlhorn, *Z. Phys.*, 1965, **187**, 21.

8 K. Siegbahn, C. Nordling, G. Johansson, J. Hedman, P. F. Héden, K. Hamrin, U. Gelius, T. Bergmark, L. O. Werme, R. Manne and Y. Baer, *ESCA Applied to Free Molecules*, North-Holland, Amsterdam, 1969.
9 L. O. Werme, T. Bergmark and K. Siegbahn, *Phys. Scr.*, 1972, **6**, 141.
10 T. A. Carlson and M. O. Krause, *Phys. Rev. Lett.*, 1966, **17**, 1079.
11 W. E. Moddeman, T. A. Carlson, M. O. Krause, B. P. Pullen, W. E. Bull and G. K. Scheitzer, *J. Chem. Phys.*, 1971, **55**, 2317.
12 J. Tulkki, T. Aberg, A. Mantykentta and H. Aksela, *Phys. Rev. A: At., Mol., Opt. Phys.*, 1992, **46**, 1357.
13 H. Pulkkinen, S. Aksela, O.-P. Sairanen, A. Hiltunen and H. Aksela, *J. Phys. B: At., Mol. Opt. Phys.*, 1996, **29**, 3033.
14 H. Aksela, S. Aksela and H. Pulkkinen, *Phys. Rev. A: At., Mol., Opt. Phys.*, 1984, **30**, 2456.
15 J. Jauhiainen, H. Aksela, S. Aksela, A. Kivimaki, O. P. Sairanen, E. Nommiste and J. Vegh, *J. Phys. B: At., Mol. Opt. Phys.*, 1995, **28**, 3831.
16 L. Partanen, M. Huttula, H. Aksela and S. Aksela, *J. Phys. B: At., Mol. Opt. Phys.*, 2007, **40**, 3795.
17 F. Tarantelli and L. S. Cederbaum, *Phys. Rev. Lett.*, 1993, **71**, 649.
18 S. Svensson, *et al.*, *Phys. Rev. Lett.*, 1994, **72**, 3021.
19 R. F. Fink, M. Kivilompolo, H. Aksela and S. Aksela, *Phys. Rev. A: At., Mol., Opt. Phys.*, 1998, **58**, 1988.
20 R. Puttner, Y. F. Hu, G. M. Bancroft, H. Aksela, E. Nommiste, J. Karvonen, A. Kivimaki and S. Aksela, *Phys. Rev. A: At., Mol., Opt. Phys.*, 1999, **59**, 4438.
21 R. Puttner, X.-J. Liu, H. Fukuzawa, T. Tanaka, M. Hoshino, H. Tanaka, J. Harries, Y. Tamenori, V. Carravetta and K. Ueda, *Chem. Phys. Lett.*, 2007, **445**, 6.
22 K. Okuyama, J. H. D. Eland and K. Kimura, *Phys. Rev. A: At., Mol., Opt. Phys.*, 1990, **41**, 4930.
23 B. Kämmerling and V. Schmidt, *Phys. Rev. Lett.*, 1991, **67**, 1848.
24 M. Neeb, J. E. Rubensson, M. Biermann and W. Eberhardt, *J. Phys. B: At., Mol. Opt. Phys.*, 1996, **29**, 43811.
25 U. Alkemper, J. Doppelfeld and F. von Busch, *Phys. Rev. A: At., Mol., Opt. Phys.*, 1997, **56**, 2741.
26 J. Viefhaus, G. Snell, R. Hentges, M. Wiedenhöft, F. Heiser, O. Geßner and U. Becker, *Phys. Rev. Lett.*, 1998, **80**, 1618.
27 J. Viefhaus, S. Cvejanovic, B. Langer, T. Lischke, G. Prumper, D. Rolles, A. V. Golovin, A. N. Grum-Grzhimailo, N. M. Kabachnik and U. Becker, *Phys. Rev. Lett.*, 2004, **92**, 083001.
28 J. Viefhaus, M. Braune, S. Korica, A. Reinkoster, D. Rolles and U. Becker, *J. Phys. B: At., Mol. Opt. Phys.*, 2005, **38**, 3885.
29 S. Ricz, A. Kover, M. Jurvansuu, D. Varga, J. Molnar and S. Aksela, *Phys. Rev. A: At., Mol., Opt. Phys.*, 2002, **65**, 042707.
30 P. Bolognesi, R. Puttner and L. Avaldi, *Chem. Phys. Lett.*, 2008, **464**, 21.
31 V. Ulrich, S. Barth, S. Joshi, T. Lischke, A. M. Bradshaw and U. Hergenhahn, *Phys. Rev. Lett.*, 2008, **100**, 143003.
32 V. Ulrich, S. Barth, S. Joshi, T. Lischke, T. Arion, M. Mucke, M. Forstel, A. M. Bradshaw and U. Hergenhahn, *J. Electron Spectrosc. Relat. Phenom.*, 2011, **183**, 70.
33 P. Lablanquie, F. Penent, R. I. Hall, H. Kjeldsen, J. H. D. Eland, A. Muehleisen, P. Pelicon, Z. Smit, M. Zitnik and F. Koike, *Phys. Rev. Lett.*, 2000, **84**, 47.
34 Y. Hikosaka, F. Penent, P. Lablanquie, R. I. Hall and K. Ito, *Meas. Sci. Technol.*, 2000, **11**, 1697.
35 P. Lablanquie, S. Sheinerman, F. Penent, R. I. Hall, M. Ahmad, Y. Hikosaka and K. Ito, *Phys. Rev. Lett.*, 2001, **87**, 053001.
36 P. Lablanquie, S. Sheinerman, F. Penent, R. I. Hall, M. Ahmad, T. Aoto, Y. Hikosaka and K. Ito, *J. Phys. B: At., Mol. Opt. Phys.*, 2002, **35**, 3265.
37 Y. Hikosaka, P. Lablanquie, F. Penent, J. G. Lambourne, R. I. Hall, T. Aoto and K. Ito, *J. Electron Spectrosc. Relat. Phenom.*, 2004, **137–140**, 287.
38 P. Lablanquie, S. Sheinerman, F. Penent, T. Aoto, Y. Hikosaka and K. Ito, *J. Phys. B: At., Mol. Opt. Phys.*, 2005, **38**, L9.
39 F. Penent, P. Lablanquie, R. I. Hall, J. Palaudoux, K. Ito, Y. Hikosaka, T. Aoto and J. H. D. Eland, *J. Electron Spectrosc. Relat. Phenom.*, 2005, **144–147**, 7.
40 K. Le Guen, M. Ahmad, D. Céolin, P. Lablanquie, C. Miron, F. Penent, P. Morin and M. Simon, *J. Chem. Phys.*, 2005, **123**, 084302.
41 S. Sheinerman, P. Lablanquie, F. Penent, J. Palaudoux, J. H. D. Eland, T. Aoto, Y. Hikosaka and K. Ito, *J. Phys. B: At., Mol. Opt. Phys.*, 2006, **39**, 1017.
42 Y. Hikosaka, P. Lablanquie, E. Shigemasa, T. Aoto and K. Ito, *J. Phys. B: At., Mol. Opt. Phys.*, 2008, **41**, 025103.
43 M. S. Schöffler, J. Titze, N. Petridis, T. Jahnke, K. Cole, L. Ph. H. Schmidt, A. Czasch, D. Akoury, O. Jagutzki, J. B. Williams, N. A. Cherepkov, S. K. Semenov, C. W. McCurdy, T. N. Rescigno, C. L. Cocke, T. Osipov, S. Lee, M. H. Prior, A. Belkacem, A. L. Landers, H. Schmidt-Böcking, Th. Weber and R. Dörner, *Science*, 2008, **320**, 920.
44 A. Cherepkov, S. K. Semenov, M. S. Schöffler, J. Titze, N. Petridis, T. Jahnke, K. Cole, L. Ph. H. Schmidt, A. Czasch, D. Akoury, O. Jagutzki, J. B. Williams, C. L. Cocke, T. Osipov, S. Lee, M. H. Prior, A. Belkacem, A. L. Landers, H. Schmidt-Böcking, Th. Weber and R. Dörner, *Phys. Rev. A: At., Mol., Opt. Phys.*, 2009, **80**, 051404R.
45 P. Kruit and F. H. Read, *J. Phys. E: Sci. Instrum.*, 1983, **16**, 313.
46 J. H. D. Eland, O. Vieuxmaire, T. Kinugawa, P. Lablanquie, R. I. Hall and F. Penent, *Phys. Rev. Lett.*, 2003, **90**, 053003.
47 F. Penent, J. Palaudoux, P. Lablanquie, L. Andric, R. Feifel and J. H. D. Eland, *Phys. Rev. Lett.*, 2005, **95**, 083002.
48 Y. Hikosaka, P. Lablanquie, F. Penent, T. Kaneyasu, E. Shigemasa, J. H. D. Eland, T. Aoto and K. Ito, *Phys. Rev. A: At., Mol., Opt. Phys.*, 2007, **76**, 032708.
49 P. Lablanquie, L. Andric, J. Palaudoux, U. Becker, M. Braune, J. Viefhaus, J. H. D. Eland and F. Penent, *J. Electron Spectrosc. Relat. Phenom.*, 2007, **156–158**, 51.
50 S. Sheinerman, P. Lablanquie, F. Penent, Y. Hikosaka, T. Kaneyasu, E. Shigemasa and K. Ito, *J. Phys. B: At., Mol. Opt. Phys.*, 2010, **43**, 115001.
51 J. Palaudoux, P. Lablanquie, L. Andric, K. Ito, E. Shigemasa, J. H. D. Eland, V. Jonauskas, S. Kucas, R. Karazija and F. Penent, *Phys. Rev. A: At., Mol., Opt. Phys.*, 2010, **82**, 043419.
52 J. Eland, C. Rigby, E. Andersson, J. Palaudoux, L. Andric, F. Penent, P. Linusson, L. Hedin, L. Karlsson, J. Rubensson, Y. Hikosaka, K. Ito, P. Lablanquie and R. Feifel, *J. Chem. Phys.*, 2010, **132**, 104311.
53 J. H. D. Eland, P. Linusson, L. Hedin, E. Andersson, J.-E. Rubensson and R. Feifel, *Chem. Phys. Lett.*, 2010, **485**, 21.
54 J. H. D. Eland, M. Hochlaf, P. Linusson, E. Andersson, L. Hedin and R. Feifel, *J. Chem. Phys.*, 2010, **132**, 014311.
55 F. Penent, P. Lablanquie, J. Palaudoux, L. Andric, G. Gamblin, Y. Hikosaka, K. Ito and S. Carniato, *Phys. Rev. Lett.*, 2011, **106**, 103002.
56 Y. Hikosaka, T. Aoto, P. Lablanquie, F. Penent, E. Shigemasa and K. Ito, *J. Phys. B: At., Mol. Opt. Phys.*, 2006, **39**, 3457.
57 T. Kaneyasu, Y. Hikosaka, E. Shigemasa, P. Lablanquie, F. Penent and K. Ito, *J. Phys. B: At., Mol. Opt. Phys.*, 2008, **41**, 135101.
58 Y. Hikosaka, T. Aoto, P. Lablanquie, F. Penent, E. Shigemasa and K. Ito, *Phys. Rev. Lett.*, 2006, **97**, 053003.
59 T. Kaneyasu, Y. Hikosaka, P. Lablanquie, F. Penent, L. Andric, G. Gamblin, J. H. D. Eland, Y. Tamenori, T. Matsushita and E. Shigemasa, *Phys. Rev. Lett.*, 2008, **101**, 183003.
60 Y. Hikosaka, P. Lablanquie, F. Penent, P. Selles, T. Kaneyasu, E. Shigemasa, J. H. D. Eland and K. Ito, *Phys. Rev. A: At., Mol., Opt. Phys.*, 2009, **80**, 031404(R).
61 P. Lablanquie, F. Penent, J. Palaudoux, L. Andric, P. Selles, S. Carniato, K. Bučar, M. Žitnik, M. Huttula, J. H. D. Eland, E. Shigemasa, K. Soejima, Y. Hikosaka, I. H. Suzuki, M. Nakano and K. Ito, *Phys. Rev. Lett.*, 2011, **106**, 063003.
62 J. H. D. Eland, M. Tashiro, P. Linusson, M. Ehara, K. Ueda and R. Feifel, *Phys. Rev. Lett.*, 2010, **105**, 213005.
63 P. Glans, R. E. La Villa, M. Ohno, S. Svensson, G. Bray, N. Wassdahl and J. Nordgren, *Phys. Rev. A: At., Mol., Opt. Phys.*, 1993, **47**, 1539.
64 G. C. King, M. Tronc, F. H. Read and R. C. Bradford, *J. Phys. B: At. Mol. Phys.*, 1977, **10**, 2479.
65 W. Mehlhorn, *Z. Phys.*, 1968, **208**, 1.
66 T. Kylli, J. Karvonen, H. Aksela, A. Kivimaki, S. Aksela, R. Camilloni, L. Avaldi, M. Coreno, M. de Simone, R. Richter, K. C. Prince and S. Stranges, *Phys. Rev. A: At., Mol., Opt. Phys.*, 1999, **59**, 4071.
67 A. G. Kochur, V. L. Sukhorukov, A. I. Dudenko and Ph. V. Demekhin, *J. Phys. B: At., Mol. Opt. Phys.*, 1995, **28**, 387.

68 S. Brunken, Ch. Gerth, B. Kanngießer, T. Luhmann, M. Richter and P. Zimmermann, *Phys. Rev. A: At., Mol., Opt. Phys.*, 2002, **65**, 042708.
69 K. G. Dyall and F. P. Larkins, *J. Phys. B: At. Mol. Phys.*, 1982, **15**, 4103.
70 K. R. Karim, M. H. Chen and B. Crasemann, *Phys. Rev. A: At., Mol., Opt. Phys.*, 1984, **29**, 2605.
71 K. R. Karim and B. Crasemann, *Phys. Rev. A: At., Mol., Opt. Phys.*, 1985, **31**, 709.
72 K. J. S. Sawhney, *et al.*, *Nucl. Instrum. Methods Phys. Res., Sect. A*, 1997, **390**, 395.
73 K. Ito, F. Penent, Y. Hikosaka, E. Shigemasa, I. H. Suzuki, J. H. D. Eland and P. Lablanquie, *Rev. Sci. Instrum.*, 2009, **80**, 123101.
74 F. A. Parpia, C. F. Fisher and I. P. Grant, *Comput. Phys. Commun.*, 1996, **94**, 249.
75 S. Fritzsche, *J. Electron Spectrosc. Relat. Phenom.*, 2001, **114–116**, 1155.
76 G. Gaigalas, T. Zalandauskas and S. Fritzsche, *Comput. Phys. Commun.*, 2004, **157**, 239.
77 S. Fritzsche, J. Nikkinen, S.-M. Huttula, H. Aksela, M. Huttula and S. Aksela, *Phys. Rev. A: At., Mol., Opt. Phys.*, 2007, **75**, 012501.
78 T. Kylli, H. Aksela, O.-P. Sairanen, A. Hiltunen and S. Aksela, *J. Phys. B: At., Mol. Opt. Phys.*, 1995, **28**, 387.
79 R. H. Dalitz, *Philos. Mag.*, 1953, **44**, 1068.
80 K. Ueda and J. H. D. Eland, *J. Phys. B: At., Mol. Opt. Phys.*, 2005, **38**, S839.
81 A. Matsuda, E. J. Takahashi and A. Hishikawa, *J. Chem. Phys.*, 2007, **127**, 114318.
82 Yu. Ralchenko, A. E. Kramida, J. Reader and NISTASD Team, NIST Atomic Spectra Database (ver. 4.0.1), [Online]. Available: http://physics.nist.gov/asd [2011]. National Institute of Standards and Technology, Gaithersburg, MD, 2010.
83 J. D. Savee, V. A. Mozhayskiy, J. E. Mann, A. I. Krylov and R. E. Continetti, *Science*, 2008, **321**, 826.
84 Y. Hikosaka, T. Kaneyasu, E. Shigemasa, P. Lablanquie, F. Penent and K. Ito, *J. Chem. Phys.*, 2007, **127**, 044305.

